NJC

Accepted Manuscript

ROYAL SOCIETY OF CHEMISTRY

www.rsc.org/njc

Cite this: DOI: 10.1039/c0xx00000x

www.rsc.org/xxxxxx

ARTICLE TYPE

Structural and electronic impact on the photophysical and biological properties of a series of Cu^I and Ag^I complexes with triphenylphosphine and pyrimidine-type thiones.

Panagiotis A. Papanikolaou,[a] Anastasios G. Papadopoulos,*[b] Eleni G. Andreadou,[c] Antonios Hatzidimitriou,[a] Philip J. Cox,[d] Anastasia A. Pantazaki[c] and Paraskevas Aslanidis*[a]*

Received (in XXX, XXX) Xth XXXXXXXXX 200X, Accepted Xth XXXXXXXXX 200X
DOI: 10.1039/b000000x

Four Cu^I and three Ag^I mixed-ligand complexes containing a heterocyclic pyrimidine-type thione (pymtH = pyrimidine-2-thione or dmpymtH = 4,6-dimethyl-pyrimidine-2-thione) and triphenylphosphine (PPh_3) have been synthesized and structurally characterized. All copper and two of the silver compounds, namely $[Cu(PPh_3)_2(pymtH)_2]BF_4$ (**1**), $[Cu(PPh_3)_3(pymtH)]BF_4$ (**2**), $[Cu(PPh_3)_2(dmpymtH)_2]BF_4$ (**3**), $[Cu(PPh_3)_3(dmpymtH)]BF_4$ (**4**), $[Ag(PPh_3)_3(pymtH)]NO_3$ (**5**) and $[Ag(PPh_3)_3(dmpymtH)]NO_3$ (**6**), reveal a tetrahedral coordination environment while $[Ag(PPh_3)_2(pymtH)]NO_3$ (**7**) preferentially adopts a trigonal planar arrangement. The stoichiometry of the isolated silver complexes does not always follow the respective stoichiometries of the synthetic procedures. The photophysical properties of all the isolated products have been evaluated. In solution, a phosphine derived emission is detected while in the solid state only $[Cu(PPh_3)_3(dmpymtH)]BF_4$ (**4**) emits from a state of different parentage. All of the complexes were also tested for in vitro antibacterial activity against four bacterial strains and for anti-inflammatory activity by measuring lipoxygenase inhibition activity.

1. Introduction

The main characteristic of *S,N*-type ligands is the combination of soft and hard sites that can selectively bind metal centers.[1a] In this sense, heterocyclic thiones are regarded as potent multifunctional donors[2] for the development of extended or higher nuclearity architectures. During the last few decades, coinage metal complexes bearing this type of ligands have attracted much research interest for their structural versatility.[1b-d,2] More precisely and because of the ability of these molecules to coordinate on the metal center in a monodentate or a bridging mode, a large variety of halogenated copper(I) and silver(I) compounds with heterocyclic thiones and aryl phosphines as auxiliary ligands have been studied, revealling in most cases a tetracoordinated mononeric or dimeric nature. Additionally, there are some examples of tricoordinated species, particularly in the presence of bulky phosphines[3,4] while bidentate P-donor ligands with small saturated carbon chains can favor the formation of dinuclear, chelated or even more sophisticated structures.[5]

On the other hand, heterocyclic thione molecules attract attention due to their relevance in biological systems.[6] In particular, the rationalization of the structural characteristics of copper-thione mixed ligand species is of significant importance in the design and understanding of analogues mimicking the blue active site of redox active cuproproteins.[7] In the same context, both copper and silver complexes containing thione and/or phosphines have revealed important antimicrobial and biological activity.[8-17] Recently, a series of Cu^I complexes incorporating heterocyclic thiones or thiolates in combination with aryl-phosphines or phenanthroline have also revealed interesting photophysical properties.[18-20] As has been shown, the emission energy of these systems can be tuned through a thione-modification related to the strength of the Cu–S bond while their emitting state is readily assigned as MLCT on the basis of both experimental and theoretical data. Further, a particular class of copper(I) systems combining thiones and phosphine moieties with intriguing photophysical properties have been reported by Yam et al.[21] The authors attributed a high energy emission located at ca. 430-550 nm in solid samples to a ligand-centered transition while in solution, a lower-lying (~ 600 nm) band with lifetime in the range of μs arising from a ^{3}LMCT excited state governs the spectrum. A similar cluster-type compound has also been reported, incorporating a sulfide ion connecting four Cu^I centers, stabilized by diphosphine bridges. In this case both solid state and fluid solution samples resulted in a long-lived yellow-orange emission assigned to a mixed LMCT/MC state.[22] Analogous luminescent copper thiolate complexes have been studied by Langer et al.[23] comprising a variety of nuclearities and core geometries. As it was reported, the core structure of these systems has a profound effect on their emissive properties which, although not clear, seem to originate from a long-lived LMCT excited state.

Continuing our investigations on the chemistry of thione-phosphine mixed-ligand coinage metal systems, we have explored the structural and photophysical properties of a series of Cu^I and Ag^I heteroleptic compounds containing the pyrimidine skeleton (pymtH = pyrimidine-2-thione and dmpymt = 4,6-dimethyl-pyrimidine-2-thione, Scheme I) in combination with triphenylphosphine (PPh_3). The complexes were all isolated as mononuclear species containing, in the case of copper, either two phosphines and two thione molecules (Cu:PPh_3:thione = 1:2:2) or

View Article Online
DOI: 10.1039/C4NJ02203C

three phosphines and one coordinated thione (Cu:PPh_3:thione = 1:3:1), depending on the reaction stoichiometry. On the other hand, silver complexes always contain one coordinated thione irrespectively of the reaction stoichiometry. Despite the detectable emission in solution, only one of the synthesized complexes emits in the solid state from a state of different parentage.

Further, we examined the antibacterial activity of all the new complexes on both Gram positive and Gram negative bacteria as well as their ability for anti-inflammatory activity by measuring lipoxygenase inhibition activity. The 5-lipoxygenase (5-LOX) pathway has been associated with a variety of inflammatory diseases including asthma, atherosclerosis, rheumatoid arthritis, pain, cancer and liver fibrosis. Several classes of 5-LOX inhibitors have been identified, but only one drug, zileuton, a redox inhibitor of 5-LOX, has been approved for clinical use.[24]

2. Results and Discussion

2.1 Synthesis

The new compounds were prepared under atmospheric conditions by mixing the respective materials in the desired equivalent amounts. In the case of copper, a binary CH_2Cl_2-MeOH solvent mixture was used while methanol was found to promote the crystallization process. In a first step $[Cu(MeCN)_4]BF_4$ is left to react in dichloromethane with the appropriate amount of PPh_3 in order to form an intermediate complex assigned as $[Cu(PPh_3)_x(MeCN)_{4-x}]BF_4$ (x = 2 or 3). Treatment of the resulting solution with the corresponding thione dissolved in methanol gives the final product. The complexes were isolated as either orange or yellow solids for the 1:2:2 or 1:3:1 stoichiometry respectively, and are microcrystalline, air stable and diamagnetic in nature. In the case of silver only methanol was used and the preparation involved the reaction of $AgNO_3$ with phosphine followed by the addition of thione dissolved in methanol. The complexes are all yellow in colour, diamagnetic and air stable. As it was revealed, the reaction of silver nitrate with PPh_3 and pymtH in a 1:2:2 ratio affords a three coordinated complex bearing only one thione and two phosphines, namely $[Ag(PPh_3)_2(pymtH)]NO_3$ (**7**) while the 1:3:1 ratio results in the expected $[Ag(PPh_3)_3(pymtH)]NO_3$ (**5**) complex. For dmpymtH, only the $[Ag(PPh_3)_3(dmpymtH)]NO_3$ (**6**) complex was isolated regardless of the reaction ratio.

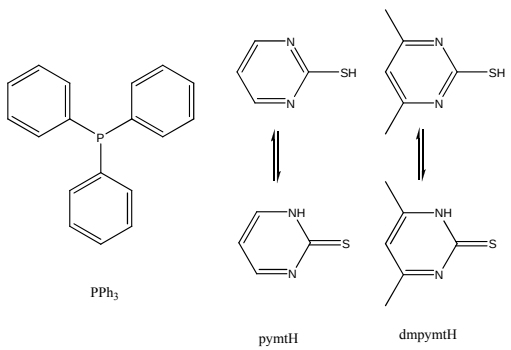

Scheme I. Molecular structure and thione-thiole tautomeric equilibria for the ligands used.

According to Scheme I, a prototropic thiol-thione tautomerism occurs for both sulfur containing ligands, although an incomplete transfer of the migrating proton between the heterocyclic nitrogen and the exocyclic sulfur atom has been suggested.[25] Several assesements of the relative stability of the two forms have revealed the prevalence of the thiol in the gas phase while, in the solid state, or in solution, the thione form appears to be more stable.[26-28] Theoretical studies on a similar system point towards a small tautomeric energy gap as a result of the competition between a thioamide resonance stabilization for the thione and a typical aromatic stabilization for the thiol.[29] The thioamide resonance could also be a potent reason for maintaining the planarity of the heterocyclic thione ring. In this framework semi-empirical calculations on the two tautomers of pyrimidine-2-thione[25] revealed a bond localization in the heterocyclic ring of the thione tautomer which points to a non- aromatic character. On the contrary the thiol form appears to be typically aromatic.

In both tautomers of pymtH and dmpymtH, coordination may occur either from the sulfur or/and the pyridine nitrogen atom of the heterocyclic ring. In the present case, X-ray crystallography shows the coordination of these ligands in the thione form as well as their monodentate interaction with the metal center through the sulfur atom. This is somewhat expected as the pre-coordinated phosphines increase the soft character of the metal predisposing the binding of the thione through its soft-base site. Considering further the stereochemical demands imposed by the bulky phosphines, the coordination of the thione through its sulfur rather than its pyridine-type nitrogen atom should also be favored because of a longer bond length which helps to reduce steric repulsions in the coordination sphere. Further, the presence of the thione form for the two ligands in the respective complexes is supported by the comparison of experimental and theoretical data for the C_{ip}–S bond length, which are in very good agreement when this tautomer is considered, as well as with literature data.[26]

2.2 Spectroscopic information

The infrared spectra of the prepared complexes show the expected distinct and strong vibrational features attributed to the phosphine moiety. These bands appear as a set of sharp peaks located around 695 and 517 cm^{-1} revealing small shifts upon coordination to the metal center.[6,30] In all cases, a strong band located in the region 1602-1610 cm^{-1} for pymtH-systems and at 1618 cm^{-1} for dmpymtH-systems can be assigned to the stretching vibrations of the –C=N– and –C=C– bonds of the thione ring. The same band appears in the free thiones at 1607 cm^{-1} and 1624 cm^{-1} for pymtH and dmpymtH, respectively, and is totally absent in the phosphine spectrum. Its negligible variation upon coordination can be attributed to changes in the electronic structure of the heterocyclic ring imposed by the presence of the metal center rather than coordination by the heterocyclic pyridinic nitrogen atoms. The latter supports the binding of the thione by the sulfur atom. Moreover, the spectra of the studied compounds contain the usual four "thioamide bands" required by the presense of the heterocyclic thione ligands in the regions ~1510, 1320, 1000 and 750 cm^{-1} [1b] overlapping partially with neighbouring peaks. In addition, the lack of ν(SH) bands at ca.

View Article Online
DOI: 10.1039/C4NJ02203C

2500-2600 cm^{-1} verifies the presence of the sulfur-ligand in its thione form although the characteristic stretching frequency of the –NH group in the 3150 cm^{-1} region[31,32] is not clearly evident. Further for the copper complexes, the BF_4^- stretching appears as a strong peak at ~1060 cm^{-1}. The nitrate absorption of the silver complexes locates around 1337 cm^{-1}.

2.3 X-ray structures

The single crystal structures of all the complexes were determined. Crystallographic data are listed in Table S1 and ORTEP views are depicted in Figures 1–7 where anions may have been removed for clarity.

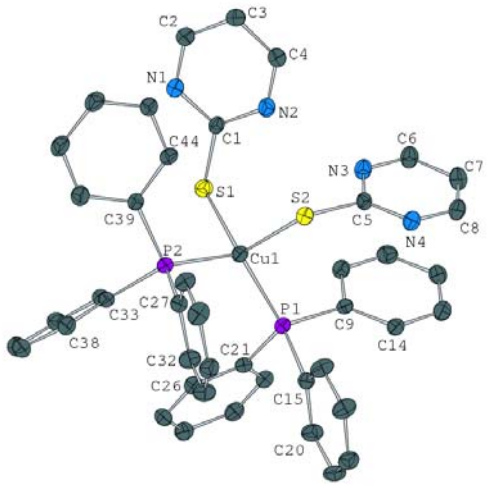

Figure 1. Perspective view of $[Cu(PPh_3)_2(pymtH)_2]BF_4$ (**1**). Selected bond lengths (Å) and angles (°): Cu1–S1=2.4093 (9), Cu1– S2=2.3658 (10), Cu1–P1= 2.2838 (9), Cu1–P2=2.2888 (9), S1–C1=1.664 (3), S2–C5=1.715 (3), S1–Cu1–S2=112.90 (3), S1–Cu1–P1=112.93 (3), S2–Cu1–P1=106.07 (3), S1–Cu1–P2=99.93 (3), S2–Cu1–P2=102.36 (4), P1–Cu1–P2=122.36 (3), Cu1–S1–C1=109.26 (11), Cu1–S2–C5=110.08 (11).

The geometrical characteristics of the copper(I) complexes **1**–**4** are comparable to those of other mononuclear copper(I) species tetrahedrally coordinated by thione and phosphine ligands. The CuP_2S_2 core geometry in **1** and **3** is very similar to that of $[Cu(py2SH)_2(PPh_3)_2]NO_3$[33] and $[Cu(py2SH)_2(PPh_3)_2]ClO_4$[34] with interbond angles around the central copper atom moderately deviating from the idealized tetrahedral geometry. The somewhat stronger distortion of the P–Cu–P angle can be accounted for by the steric hindrance induced by the bulky phenyl-rings of the two phosphine units. In this respect the tetrahedral arrangement in **2** and **4**, each with three bulky phosphine ligands, appears to be somewhat more regular as in **1** and **3**.

Considering the bond distances, the most remarkable feature in the structures of **1** and **3** is the quite large asymmetry in the two individual Cu–S bond distances. Further, the Cu–P bonds in **2** and **4** are clearly larger than those in **1** and **3**, probably due to steric effects.

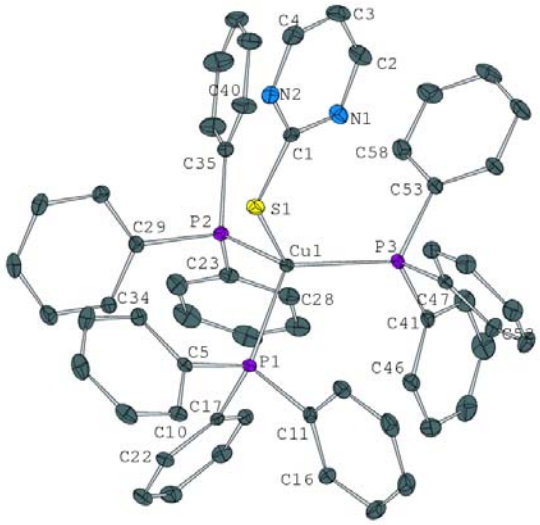

Figure 2. Perspective view of $[Cu(PPh_3)_3(pymtH)]BF_4$ (**2**). Selected bond lengths (Å) and angles (°): Cu1–S1=2.3902 (12), Cu1– P1=2.3648 (11), Cu1–P2= 2.3726 (12), Cu1–P3=2.3334 (11), S1–C1=1.691 (4), S1–Cu1–P1=95.17 (4), P1–Cu1–P2=107.85 (4), P1–Cu1–P3=113.37 (4), S1–Cu1–P2=109.43 (5), S1–Cu1–P3=110.78 (4), P2–Cu1–P3=117.86 (4), Cu1–S1–C1=113.99 (16).

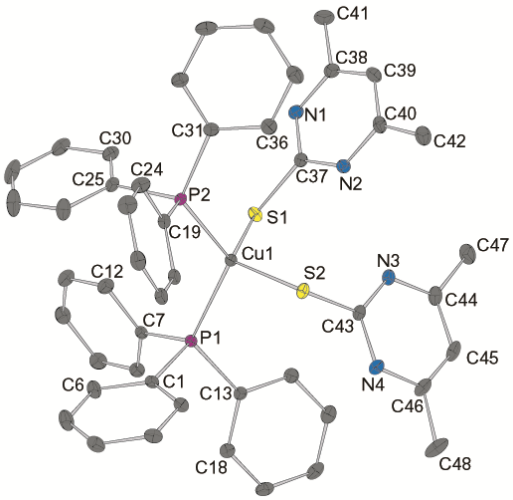

Figure 3. Perspective view of $[Cu(PPh_3)_2(dmpymtH)_2]BF_4$ (**3**). Selected bond lengths (Å) and angles (°): Cu1–S1=2.3350 (6), Cu1– S2=2.3815 (6), Cu1–P1= 2.3013 (5), Cu1–P2=2.2958 (5), S1–C37=1.711 (2), S2–C43=1.700 (2), S1–Cu1–S2=119.434 (11), S1–Cu1–P1=101.24 (2), S2–Cu1–P1=105.17 (2), S1–Cu1–P2=108.38 (2), S2–Cu1–P2=102.75 (2), P1–Cu1–P2=120.97 (2), Cu1–S1–C37=112.70 (7), Cu1–S2–C43=110.03 (7).

Similar to the copper complexes discussed above, the silver nucleus in $[Ag(PPh_3)_3(pymtH)]NO_3$ (**5**) and $[Ag(PPh_3)_3(dmpymtH)]NO_3$ (**6**) is tetracoordinated with a P_3S ligand donor set. It is noteworthy that our previous studies with thione/triphenylphosphine mixed-ligand complexes of silver(I) show that $AgNO_3$ preferentially forms compounds with a AgP_2S_2 central core.[1d,35]

View Article Online
DOI: 10.1039/C4NJ02205C

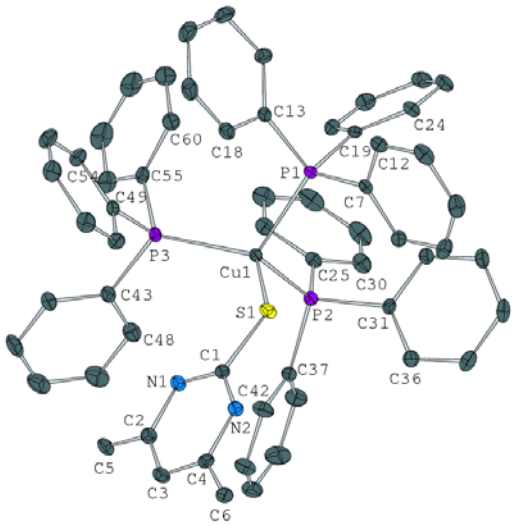

Figure 4. Perspective view of $[Cu(PPh_3)_3(dmpymtH)]BF_4$ (**4**). Selected bond lengths (Å) and angles (°): Cu1–S1=2.3736 (11), Cu1– P1=2.3769 (10), Cu1–P2= 2.3698 (11), Cu1–P3=2.3418 (10), S1–C1=1.711 (4), S1–Cu1–P1=93.83 (4), P1–Cu1–P2=108.13 (4), P1–Cu1–P3=113.80 (4), S1–Cu1–P2=110.84 (4), S1–Cu1–P3=111.55 (4), P2–Cu1–P3=116.42 (4), Cu1–S1–C1=115.42 (13).

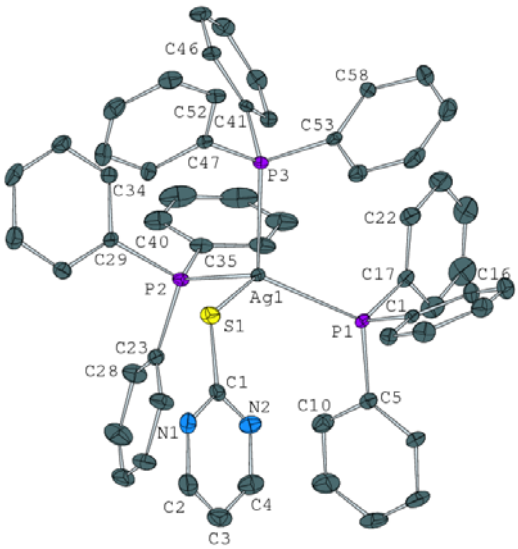

Figure 5. A view of $[Ag(PPh_3)_3(pymtH)]NO_3$ (**5**). Selected bond lengths (Å) and angles (°): Ag1–S1=2.6310 (9), Ag1–P1=2.5054 (8), Ag1–P2= 2.5349 (9), Ag1–P3=2.5626 (8), S1–C1=1.681 (4), S1–Ag1–P1=109.30 (3), S1–Ag1–P2=111.78 (3), S1–Ag1–P3=94.44 (3), P1–Ag1–P2=119.49 (3), P1–Ag1–P3=113.27 (3), P2–Ag1–P3=105.73 (3), Ag1–S1–C1=108.78 (13).

A comparison of the structures of **5** and **6** with those of the corresponding copper counterparts **2** and **4** reveals an overall less extented divergence of the interbond angles from the ideal tetrahedral value, suggesting a better rearrangement of the bulky ligands around the bigger silver cation. In both structures the non-protonated nitrogen atom of the thione ligand is oriented towards the metal center but the distance between the two atoms (3.552 Å in **5** and 4.795 Å in **6**) is too large to warrant any kind of bonding interaction.

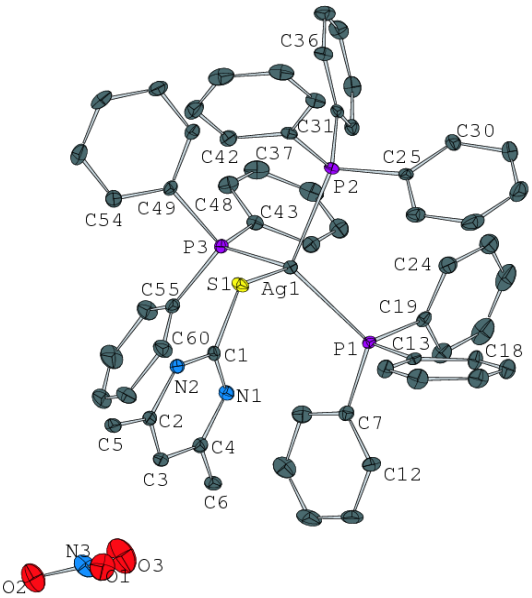

Figure 6. A view of $[Ag(PPh_3)_3(dmpymtH)]NO_3$ (**6**). Selected bond lengths (Å) and angles (°): Ag1–S1=2.6052 (11), Ag1–P1=2.5228 (10), Ag1–P2= 2.5881 (10), Ag1–P3=2.5370 (11), S1–C1=1.695 (4), S1–Ag1–P1=109.92 (4), S1–Ag1–P2=91.65 (4), S1–Ag1–P3=115.93 (4), P1–Ag1–P2=113.67 (4), P1–Ag1–P3=106.38 (4), P2–Ag1–P3=106.38 (4), Ag1–S1–C1=108.73 (15).

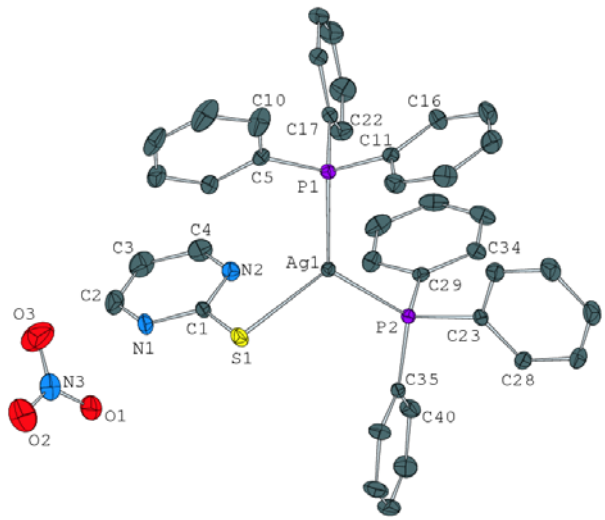

Figure 7. A view of $[Ag(PPh_3)_2(pymtH)]NO_3$ (**7**). Selected bond lengths (Å) and angles (°): Ag1–S1=2.5701 (5), Ag1–P1=2.4480 (5), Ag1–P2= 2.4415 (4), S1–C1=1.680 (2), S1–Ag1–P1=118.603 (18), S1–Ag1–P2=113.294 (18), P1–Ag1–P2=127.817 (16), Ag1–S1–C1=89.34 (6).

Compound **7** has been synthesized and characterized earlier in the context of a study on mixed-ligand silver(I) compounds of various heterocyclic thiones and its crystal structure is already known.[36a] However, for the sake of completeness, we consider it useful to include this compound in our present investigations.

The AgP_2S core in **7** is nearly planar with interbond angles deviating slightly from the idealized value of 120°. As will be

View Article Online
DOI: 10.1039/C4NJ02203C

shown further below, the exceptional formation of a tricoordinate complex originates from electronic rather than from steric factors. At this point it should be mentioned that the experimentally determined distance of 2.737 Å between the non-protonated N-atom of the pymtH ligand and the metal ion, lies out of the statistical upper limit of 2.72 Å already reported for a weak interaction between Ag^I and light donor atoms[36b] and thus typically excludes an even weak Ag-N bonding. This is evident also from the retaining of an almost ideal trigonal planar arrangement of the cation while in the case of a fourth, even weak, metal-pymtH interaction, a perceptible deformation towards a tetrahedral stucture should be expected. Further, the shorter metal-ligand bond lengths in **7** compared to **5** agree with a more profound sp^2 character for the metal center. The deviation of the electronic structure of the cation from the 18e rule can be related to a substantial charge accumulation on the silver core as it results from DFT calculations (vide infra).

2.4 Photophysical studies

The electronic absorption spectra of all complexes in dichloromethane reveal a strong band in the ultraviolet region and a lower energy shoulder extending up to 430 or 480 nm for the silver and copper derivatives, respectively (Figure 8 and Figure S1). The high intensity peak can be assigned to intraligand π-π^* transitions of the aromatic rings while the broad low-lying absorption, located in the region of the free thiones chromophoric band, can be assigned to a combination of thione intraligand and charge transfer excitations (Figure S2). The charge transfer nature

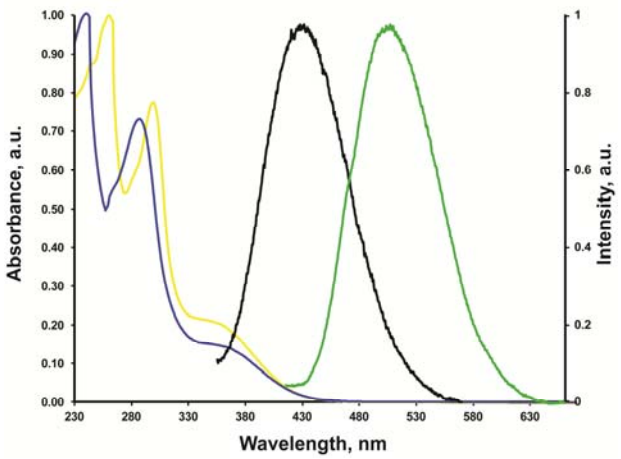

Figure 8. Normalized absorption spectra of $[Cu(PPh_3)_2(dmpymtH)_2]BF_4$ (**3**) (blue) and $[Cu(PPh_3)_3(dmpymtH)]BF_4$ (**4**) (yellow) in dichloromethane. Normalized emission spectrum of PPh_3 (black) and $[Cu(PPh_3)_3(dmpymtH)]BF_4$ (**4**) (green) in KBr disk after photoexcitation at 300 nm and 350 nm respectively.

is supported by the calculated ε values reported in Table 1. Because of the phosphine propensity to act as an electron donor,[7d] the CT transitions involve a charge displacement from the latter moiety or the central metal region towards the acceptor empty π-orbitals of the heterocyclic thione unit (MLCT/LLCT).[37-39] The MLCT character of the chromophoric absorption agrees well with the blueshift observed for silver compared to copper complexes. In the case of the Cu^I ion, such transitions are favored by its strong reducing nature while the redox inertness of Ag^I does not allow for similar low-energy electronic excitations.[40] Also, the absorption of the dmpymtH-systems is slightly blueshifted compared to the respective pymtH-compound, as shown in Table 1. This can be assigned to the destabilization of the accepting thione-orbitals through a positive inductive effect imposed by the methyl groups of the pyrimidine ring.

All of the synthesized compounds were tested for their ability to emit both in the solid sate and in solution. After excitation in the UV region (λ_{exc} = 300 nm) of an optically dilluted sample of each complex in dichloromethane, a broad peak maximizing around 480 nm is detected (Figure S3). This emission is not observed when the samples are excited at longer wavelengths (λ_{exc} > 350 nm) indicating that it results from a higher lying excited state of the complexes. The appearance of this emission in the same wavelength both for copper and silver complexes typically excludes a MLCT character because of the aforementioned different susceptibility of the two metals towards oxidation. Additionally, the retaining of the emission in acetonitrile, as has been observed, points against the MLCT character for the emissive state. On the other hand and supposing an effective steric protection of the metal center by the coordinated phosphines, the emission energy of the complexes accommodating three such ligands should be higher compared to the rest of the systems. This is due to a more crowded coordination sphere which would prevent structural rearrangements and the stabilization of the excited state through exciplex formation.[41a] Under the same excitation (300 nm), a similar emission band is observed in a dichloromethane solution of triphenylphosphine[41b] indicating that the emitting state of the complexes can be readily assigned as IL-PPh_3 in nature (Figure S3) or stemming from an uncoordinated phosphine moiety because of a partial dissociation.

Table 1. Photophysical data of the synthesized Cu^I and Ag^I complexes in the solid state and in dichloromethane.

Compound	λ_{abs}, nm[a] (ε_{abs}, $dm^3mol^{-1}cm^{-1}$)	λ_{em}, nm[b,c]	λ_{em}, nm[d]
$[Cu(PPh_3)_2(pymtH)_2]BF_4$ (**1**)	364(sh) (7331)	473	-
$[Cu(PPh_3)_3(pymtH)]BF_4$ (**2**)	354(sh) (3590)	480	-
$[Cu(PPh_3)_2(dmpymtH)_2]BF_4$ (**3**)	357(sh) (6516)	478	-
$[Cu(PPh_3)_3(dmpymtH)]BF_4$ (**4**)	352(sh) (2829)	479	505
$[Ag(PPh_3)_2(pymtH)]NO_3$ (**5**)	351(sh) (3473)	484	-
$[Ag(PPh_3)_3(pymtH)]NO_3$ (**6**)	349(sh) (2565)	487	-
$[Ag(PPh_3)_3(dmpymtH)]NO_3$ (**7**)	347 (3765)	473	-

[a]refers to the longest wavelength absorption in dichloromethane
[b]λ_{exc} = 300 nm, [c]dichloromethane solution, [d]KBr disk

In the case of the free thiones in dichloromethane, only dmpymtH was shown to luminesce (λ_{exc} = 350 nm) with a

View Article Online
DOI: 10.1039/C4NJ02203C

maximum at 530 nm (Figure S2) while in the solid state, no appreciable emission was detected for pymtH or dmpymtH. On the other hand, triphenylphosphine exhibits a broad band with maximum at 428 nm after photoexcitation at 300 nm in KBr (Figure 8). Concerning the metal complexes in the solid state, only $[Cu(PPh_3)_3(dmpymtH)]BF_4$ (**4**) luminesces (λ_{exc} = 350 nm) with a strong and broad emission located at 505 nm (Figure 1). By considering the similar photophysical behavior of the phosphine and this complex in solution, the observed emission of the latter in the solid state should be of a different parentage to the one detected in dichloromethane. This can be ascribed to a lower lying MLCT excited state, further supported by theoretical data (see further below) as well as by the fact that the selected excitation cannot populate any IL-phosphine-based excited states. Additionally, the emission of the complex in the solid state appears to be redshifted compared to the one observed in solution. Since in the solid state energy loses are reduced because of a more rigid environment, the lower emission energy of the solid form can be assigned respectively to a lower energy emitting state compared to solution. As already reported[18-20] similar assignments concerning the character of the emissive state have been reported. In the present case, the steric bulkiness of $[Cu(PPh_3)_3(dmpymtH)]BF_4$ (**4**) accounts for the narrow Stokes shift. On the other hand and compared to the typical $[Cu(NN)_2]^+$- and $[Cu(NN)(PP)]^+$-type chromophores,[7d,41] the coordination of solely soft bases on the metal center can justify the relatively high energy absorption and emission bands, through stabilization of the Cu^I oxidation state.

The $[Cu(PPh_3)_3(dmpymtH)]BF_4$ (**4**) complex presents the same structural characteristics with the one reported by Langer et al.[23] bearing two independent Cu^I centers. In both cases, each metal core is coordinated by three phosphorus and one sulfur atom resulting to the same CuP_3S-type chromophore. Additionally, and as in our case, the dinuclear complex of Langer et al,.[23] does not emit in solution after photoexcitation in the visible region while this compound and $[Cu(PPh_3)_3(dmpymtH)]BF_4$ (**4**) both emit in the solid state at the same wavelength (505 nm). Further, and according to reference data, Langer et al., attribute the emission of the dinuclear complex to a longlived LMCT state related to the strong electron-donating ability of the coordinated thiolate. On the other hand, such states are known to be generally non-emissive,[41] while, in $[Cu(PPh_3)_3(dmpymtH)]BF_4$ (**4**) the thione ligand is accomodated in its neutral form thus limiting its donor ability. In our opinion and based on DFT results presented below, it is safer to attribute the solid state emission of $[Cu(PPh_3)_3(dmpymtH)]BF_4$ (**4**) to an MLCT state. The lack of lifetime data do not allow for a clear assignement of the total spin although the participation of a ^{3}MLCT is largely expected. The emission is quenched in solution either by air oxygen or structural rearrangements after photoexcitation.

2.5 Evaluation of antibacterial activity

The antimicrobial activities of the complexes **1-7** (average of three measurements) were estimated by monitoring the growth of certain Gram-positive (*B. subtilis, B. cereus, S. aureus*) and Gram-negative (*E. coli*) bacterial srtains in the presence of various concentrations of these complexes, ranging from 0 to 100 $\mu g \cdot mL^{-1}$. The minimum inhibitory concentration (MIC) values obtained for each strain and each compound are presented in Table 2.

Table 2 Antimicrobial activities of the complexes **1-7** evaluated by the inhibitory concentration 50 ($\mu g\ mL^{-1}$).

Compound	*E. coli* (-)	*S. aureus* (+)	*B. cereus* (+)	*B. subtilis* (+)
	IC_{50} (μg/mL)	IC_{50} (μg/mL)	IC_{50} (μg/mL)	IC_{50} (μg/mL)
$[Cu(MeCN)_4]BF_4$	>100	28	>100	>100
$[Cu(PPh_3)_2(pymtH)_2]BF_4$ (**1**)	-	-	-	-
$[Cu(PPh_3)_3(pymtH)]BF_4$ (**2**)	-	24	26	-
$[Cu(PPh_3)_2(dmpymtH)_2]BF_4$ (**3**)	-	13	-	-
$[Cu(PPh_3)_3(dmpymtH)]BF_4$ (**4**)	-	12	24	12
$[Ag(PPh_3)_3(pymtH)]NO_3$ (**5**)	7.5	8	8	9
$[Ag(PPh_3)_3(dmpymtH)]NO_3$ (**6**)	3.5	9	8	10
$[Ag(PPh_3)_2(pymtH)]NO_3$ (**7**)	25	17	24	18

Among the three silver compounds, excellent antibacterial activity is observed for the tetrahedral complexes **5** and **6**, while the effectiveness of the trigonal planar one (compound **7**) is much less pronounced.

Contrary to that, the antibacterial activities of the four copper(I) complexes **1**–**4** are quite different. Thus, while compound **1** is found to be inactive, the other three show selective antibacterial activity only against certain types of Gram-positive bacteria strains. In particular, $[Cu(PPh_3)_3(dmpmt)]BF_4$ (compound **4**) exhibits significant antibacterial activity against all three Gram-positive bacteria strains, with a particularly low IC_{50} value of 12 $\mu g \cdot mL^{-1}$ against *S. aureus* and *B. subtilis*, while $[Cu(PPh_3)_2(dmpymtH)_2]BF_4$ (compound **3**) displays an equally good activity only against *S. aureus*. It should be noted that no antibacterial activity was detected for the free pymtH, dmpymtH and PPh_3 used as ligands.

2.6 *In vitro* anti-inflammatory activity

Lipoxygenases (LOX) catalyse the regio- and stereo-specific dioxygenation of polyunsaturated fatty acids containing 1(Z), 4(Z) pentadiene system, to form hydroperoxides, which are leukotriene precursors. The dioxygenase activity of LOX displays rather broad substrate specificity. The inhibitory concentration (IC_{50}) values of the tested compounds, and nordihydroguaiaretic acid (NDGA) towards soybean LOX after 7 min of incubation are given in Table 3 and the effect of concentration on lipoxygenase inhibition activity for the $[Cu(PPh_3)_2(pymtH)_2]BF_4$ (**1**) is depicted in Figure 9.

Screening of the anti-inflammatory activity of the complexes under investigation showed that most of them exhibited a moderate inhibition of lipoxygenase activity with the exception of $[Cu(PPh_3)_2(pymtH)_2]BF_4$ (**1**), which, with an IC_{50} of 176 μM, is the most prominent inhibitor among the evaluated compounds.

View Article Online
DOI: 10.1039/C4NJ02203C

Table 3. *In vitro* evaluation of anti-inflammatory activity based on lipoxygenase activity inhibition.

Compound	Inhibition of lipoxygenase activity IC_{50} (μM)
$[Cu(MeCN)_4]BF_4$	440
$[Cu(PPh_3)_2(pymtH)_2]BF_4$ (**1**)	176
$[Cu(PPh_3)_3(pymtH)]BF_4$ (**2**)	> 500
$[Cu(PPh_3)_2(dmpymtH)_2]BF_4$ (**3**)	360
$[Cu(PPh_3)_3(dmpymtH)]BF_4$ (**4**)	> 500
$[Ag(PPh_3)_3(pymtH)]NO_3$ (**5**)	460
$[Ag(PPh_3)_3(dmpymtH)]NO_3$ (**6**)	> 500
$[Ag(PPh_3)_2(pymtH)]NO_3$ (**7**)	247.25
NDGA	1.3

Among the silver (I) complexes, $[Ag(PPh_3)_2(pymtH)]NO_3$ (**7**) displayed the most potent inhibition on lipoxygenase activity. This finding might be related to the number of PPh_3 moieties present in each case. The same effect was obtained among the copper (I) compounds, where again the strongest activity was found for complexes **1** and **3**, also possessing only two PPh_3 ligands. Thus, this result suggests that the bulkiness of the third PPh_3 turns probably the compounds less accessible to the active site or generally to the surface of the enzyme lipoxygenase in order to inhibit effectively the enzyme.

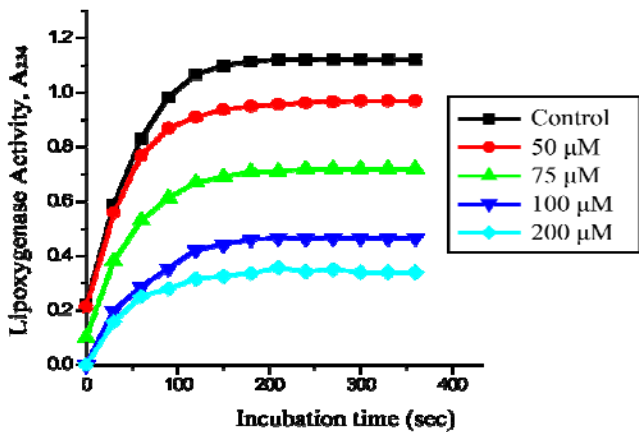

Figure 9. Effects of various concentrations of $[Cu(PPh_3)_2(pymtH)_2]BF_4$ (**1**) on lipoxygenase inhibition activity.

2.7 Theoretical Results

2.7.1 Geometrical features

In order to understand some marked structural and electronic features of the compounds under study we performed DFT calculations on the free thiones and the respective cationic complexes. The PBE1PBE[43] functional was selected along with the SDD[44] basis set for the description of the metal core and the 6-31G(d)[45] basis sets for light atoms. The structure of the two ligands was optimized both in the thione and the thiol form either in the gas phase or in solution. In the latter case a rather nonpolar solvent (dicloromethane) or a solvent of medium polarity (methanol) was considered. The obtained geometrical and energetic parameters for the two forms in the assumed media are summarized in Table S2. Despite the fact that for the isolated ligands in the vacuum state the thiol form appears to be more stable (by 2.8 kcal mol^{-1} for pymtH and 1.4 kcal mol^{-1} for dmpymtH), in solution the two molecules adopt their thione form. This is more stable than the thiol tautomer by ca. 7.2 kcal mol^{-1} in dichloromethane and 8.6 kcal mol^{-1} in methanol both for pymtH and dmpymtH. Consequently, it is expected that in the solvent system used for the preparation of the present complexes, the sulfur-containing ligands will mainly occur in their thione form in agreement with the solid state experimental as well as previously reported[26-28] findings.

An intriguing point is related to the stoichiometry of the resulting Ag^I compounds. In all of the Cu^I complexes the respective ligands are accommodated in the isolated structures in accordance to the molecular ratios used in the synthetic procedure. However, treatment of two equivalents of triphenylphosphine with one equivalent of silver salt and two equivalents of pymtH yields the tricoordinated trigonal planar $[Ag(PPh_3)_2(pymtH)]^+$ (**7**) complex instead of the expected $[Ag(PPh_3)_2(pymtH)_2]^+$ complex. Similarly, the reaction of $AgNO_3$ with dmpymtH and PPh_3 results to the formation of the tetrahedral $[Ag(PPh_3)_3(dmpymtH)]^+$ (**6**) cation irrespectively of the reaction stoichiometry. In order to explore the reasons leading to this irregular behavior we optimized the structures of both the isolated and the expected systems containing the sulfur ligands in their thione form. Analogous calculations for the isolated Cu^I complexes were also performed. Since in this case no differentiations in the reaction products were observed, the obtained results will be only discussed briefly and in line with the respective silver compounds.

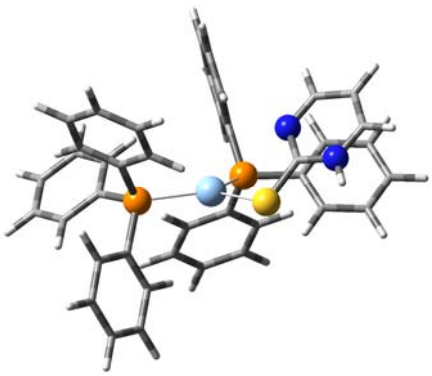

Figure 10. Optimized structure of the trigonal planar $[Ag(PPh_3)_2(pymtH)]^+$ (**7**) cation revealing the non-favoring orientation of the heterocyclic pyridine-type N atom for coordination on the metal center.

View Article Online
DOI: 10.1039/C4NJ02205C

Geometrical parameters of the studied Ag^I cations are given in Tables S3 and S4. After optimization the three-coordinated complex retains its trigonal planar configuration with a slight deviation of the sulfur atom from the plane defined by the two phosphorus atoms and the metal center amounting to 0.106 Å and two slightly unequivalent P–Ag–S angles of 114.4° and 113.1°. The two Ag–P bond lengths also show a small difference probably assigned to strereochemical demands resulting from the orientation of the pyrimidine ring towards one of the coordinated phosphines in the optimized structure. Both of these bond lengths as well as that of the Ag–S bond (2.598 Å) are in good agreement with experimental data. On the other hand, the distance of the metal ion from the heterocyclic pyridine-type nitrogen atom is found at 3.261 Å precluding any strong bonding interaction between the two centers (Figure 10). As can be seen by the comparison of geometrical data for the optimized structure of pymtH in the vacuum state and the respective $[Ag(PPh_3)_2(pymtH)]^+$ (**7**) complex (Tables S2 and S3 respectively), the coordination of the thione to the metal ion through the exocyclic sulfur atom does not impose any severe structural distortions to the heterocyclic ring resulting only in a weak shortening of the C_{ip}–N_{pyr} and C_{ip}–N_{im} bond lengths while an elongation of about 0.025 Å occurs for the C_{ip}–S bond, related to the charge displacement towards the metal upon ligation.

Coordination of two pymtH and two PPh_3 moieties on the Ag^I cation towards the expected $[Ag(PPh_3)_2(pymtH)_2]^+$ complex results to an optimized tetrahedral arrangement around the metal center (Table S3). The two Ag–S and the two Ag–P bond lengths differ by 0.008 Å and 0.034 Å respectively while the P–Ag–P bond angle appears sustantially larger compared to the respective S–Ag–P angles. An apparent difference also occurs in the bond angles defined by each phosphorus atom, the silver core and each of the two sulfur centers. The dihedral angle between the two P–Ag–P and S–Ag–S planes is defined at 84.26°. As in the trigonal system no strong structural changes are observed on the thione ring upon coordination with an elongation of the C_{ip}–S bonds of ca. 0.05 Å. Similarly coordination of three phosphines and one pymtH molecule on the silver cation favours a tetrahedral AgP_3S chromophore unit isolated experimentally in the form of $[Ag(PPh_3)_3(pymtH)]^+$ (**5**). The optimized structure (Table S3) reveals three slightly different Ag–P bond lengths with P–Ag–P bond angles varying between ca. 113° and 120°. The Ag–S bond distance adopts a larger value compared to the two former cases partially due to stereochemical repulsions stemming from the phosphines. The difference of 0.189 Å observed for $[Ag(PPh_3)_2(pymtH)]^+$ (**7**) and $[Ag(PPh_3)_3(pymtH)]^+$ (**5**) indicates a weaker coordination of the thione in the latter system although this is not shown by the C_{ip}–S bonds which are approximately equal in length.

As mentioned above, reaction of dmpymtH with $AgNO_3$ and PPh_3 always results in the isolation of the tetrahedral $[Ag(PPh_3)_3(dmpymtH)]^+$ (**6**) complex. The nature of this cation as well as that of the expected $[Ag(PPh_3)_2(dmpymtH)_2]^+$ complex were also investigated by DFT calculations. Structural data of the two optimized structures are given in Table S4. The elusive $[Ag(PPh_3)_2(dmpymtH)_2]^+$ species adopts a tetrahedral coordination environment comprising two almost equivalent Ag–S and Ag–P bond lengths respectively, while the P-Ag-P bond angle is by ~7° larger compared to the largest value of the S–Ag–P angles. This can be assigned to steric repulsions exerted between the bulky phosphines although the presence of the methyl groups on the thione rings restricts the distance between the two PPh_3 ligands compared to the respective pymtH complex. The dihedral angle defined by the P–Ag–P and S–Ag–S planes amounts to 77.12° while upon coordination a minor elongation of the C_{ip}–S bonds (~ 0.06 Å) is assigned to the coordination of the sulfur atoms on the metal center. An analogous tetrahedral geometry is obtained after optimization of the isolated $[Ag(PPh_3)_3(dmpymtH)]^+$ (**6**) cation. In contrast to what is observed in the respective pymtH complexes, the Ag–S bond length in the present case is shorter by 0.03 Å than the one found in the $[Ag(PPh_3)_2(dmpymtH)_2]^+$. Nevertheless and despite the stronger Ag–S interaction as expressed through the bond lengths, the C_{ip}–S bond of the present complex appears to be also shortened compared to the respective bonds in $[Ag(PPh_3)_2(dmpymtH)_2]^+$. Further the three Ag–P bonds are almost of equal length and P–Ag–P bond angles vary from ca. 110° to 118°.

2.7.2 Energetic assignments

In order to investigate the aforementioned irrational behavior of the reactions involving silver, we proceeded to estimate the thermodynamic stability of the various products. According to thermochemical results for the reaction of Ag^I with pymtH, the formation of tetrahedral $[Ag(PPh_3)_2(pymtH)_2]^+$ is thermodynamically more favored with computed reaction heats, $\Delta_R H$, of -128.17 kcal mol^{-1} for the trigonal complex and -144.76 kcal mol^{-1} for the tetrahedral complex. The same term for $[Ag(PPh_3)_3(pymtH)]^+$ (**5**) is estimated at -133.17 kcal mol^{-1}. As far as it concerns the Ag^I-dmpymtH systems, formation of $[Ag(PPh_3)_2(dmpymtH)_2]^+$ is favored by ca. 10.75 kcal mol^{-1} over $[Ag(PPh_3)_3(dmpymtH)]^+$ (**6**) ($\Delta_R H$ = -147.77 and -137.02 kcal mol^{-1} respectively). Accordingly, although not isolated experimentally, the Ag:PPh_3:thione = 1:2:2 cation appears to be thermodynamically more preferable for both thione ligands. Despite the inefficiency of thermochemical calculations to rationalize the formation of the observed silver products, the data are sufficient to explain the difference on the Ag:PPh_3:thione = 1:2:2 reaction ratio product formation for the two thiones. More precisely and for the above analogy, dmpymtH leads to the formation of the tetrahedral $[Ag(PPh_3)_3(dmpymtH)]^+$ (**6**). When pymtH is used instead, trigonal $[Ag(PPh_3)_2(pymtH)]^+$ (**7**) complex is isolated which appears to be 5 kcal mol^{-1} less stable than the respective $[Ag(PPh_3)_3(pymtH)]^+$ (**5**) complex. As the estimated difference lies on the limit of thermal energy (3-6 kcal mol^{-1}) stereochemical factors in the coordination shpere are expected to govern the final product formation thus leading to a less crowded trigonal planar conformation. In the case of dmpymtH, the same energy difference accounts for the isolation of the more crowded tetrahedral $[Ag(PPh_3)_3(dmpymtH)]^+$ (**6**) complex which appears to be 110.59 kcal mol^{-1} more stable than the respective trigonal $[Ag(PPh_3)_2(dmpymtH)]^+$ complex ($\Delta_R H$ for the latter been estimated at only -26.43 kcal mol^{-1}).

Analogous findings are obtained by including entropic factors in the above study. Further, in the case of copper, the calculated

View Article Online
DOI: 10.1039/C4NJ02203C

thermochemical data are in agreement with the isolation of $[Cu(PPh_3)_2(pymtH)_2]^+$ (**1**) and $[Cu(PPh_3)_2(dmpymtH)_2]^+$ (**3**) for a Cu:PPh_3:thione = 1:2:2 reaction stoichiometry. The divergent coordination behavior of silver, especially underlined by the formation of a trigonal planar geometry, agrees with its known high lability demonstrated in a variety of disproportionation and ligand scrambling reactions.[46]

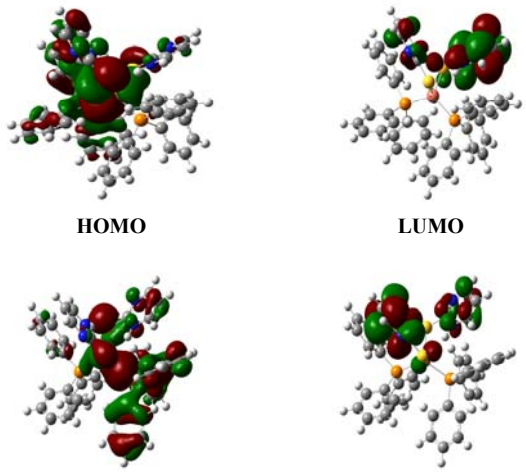

Figure 11. Selected FMOs of the $[Cu(PPh_3)_2(pymtH)_2]^+$ (**1**) cation.

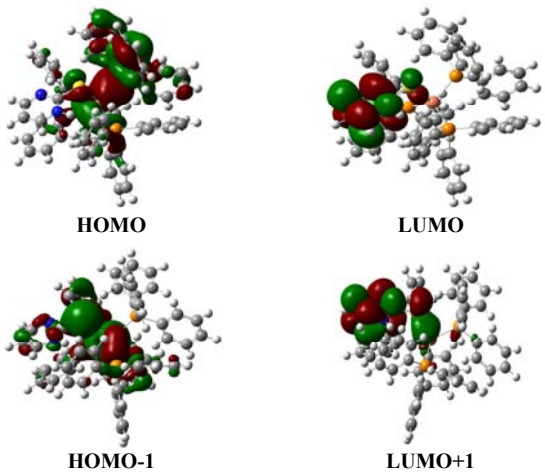

Figure 12. Selected FMOs of the $[Cu(PPh_3)_3(pymtH)]^+$ (**2**) cation.

By inspecting the NBO atomic charges of the Ag^I-pymtH related systems (Table S7), it becomes obvious that upon coordination there is a charge shift from the sulfur atom (-0.16 charge units for the free thione) and the two phosphorus atoms (+0.91 charge units in the free triphenylphosphine) towards the metal center (-0.13 charge units for the S and +0.95 charge units for the P atoms in the complex) with the latter aquiring a charge of +0.29 units in the $[Ag(PPh_3)_2(pymtH)]^+$ (**7**) complex. An analogous diminishing of electronic charge occurs for the iminic nitrogen atom of the thione upon coordination (from -0.56 in the free thione to -0.54 in the Ag^I-complex) while an opposite sign charge variation of ca. -0.02 units is observed for the pyridine-type nitrogen atom (q_{Npyr} = -0.46 in the free thione and -0.48 in the complex). The latter finding denotes the lack of a Ag^I–N_{pyr} coordination interaction in the complex. In this respect the preference for a trigonal planar Ag^I-pymtH complex over the respective tetrahedral $[Ag(PPh_3)_2(pymtH)_2]^+$ complex cannot be attributed to an elusive Ag^I –N_{pyr} bonding interaction which could block the ligation of a second pymtH species. In the same context the isolation of the tetrahedral $[Ag(PPh_3)_3(pymtH)]^+$ (**5**) complex accounts for the propensity of the $[Ag(PPh_3)_2(pymtH)]^+$ (**7**) unit to accommodate a fourth ligand. Since PPh_3 is bulkier than pymtH, steric factors are quite unlikely to be held responsible for preventing the formation of the $[Ag(PPh_3)_2(pymtH)_2]^+$ entity.

In the optimized structure of the expected $[Ag(PPh_3)_2(pymtH)_2]^+$ complex (Table S3), the two N_{pyr} atoms are directed away from the metal core excluding any bonding interaction while they retain the same charge as in the free thione. A substantial electron density accumulation is observed on the central atom which now appears with a minor positive charge of +0.019 charge units. This could be rationalized on the basis of a less efficient π-back donation towards the heterocyclic thione ring compared to the trigonal planar system.[36a] By considering the $[Ag(PPh_3)_2]^+$ fragment as the acceptor and pymtH as the donor moiety upon coordination, a CDA[47] analysis of the two structures indeed reveals a larger back electron transfer (b) per thione ligand in the case of the $[Ag(PPh_3)_2(pymtH)]^+$ (**7**) complex (b = 0.296 vs 0.223 units). This in conjunction to a less crowded stereochemical environment in the coordination sphere and a more profound Ag–S electrostatic interaction as shown by the calculated atomic charges, could support the formation of the trigonal planar $[Ag(PPh_3)_2(pymtH)]^+$ (**7**) complex in preference to the respective tetrahedral $[Ag(PPh_3)_2(pymtH)_2]^+$ complex. In the same context, the uptake of an additional phosphine from the Ag^I center in order to form the highly crowded $[Ag(PPh_3)_3(pymtH)]^+$ (**5**) complex can be related to an even stronger π-back donation towards the thione ligand (b = 0.323) as well as to an effective Ag–S electrostatic interaction according to atomic charges. The weaker π-back transfer to each pymtH moiety in $[Ag(PPh_3)_2(pymtH)_2]^+$ is well exemplified by the equal delocalization of either of LUMO and LUMO+1 over both these units while in the rest of the complexes comprising two coordinated thiones, each of the lowest virtual orbitals is mainly confined to only one thione (see Table S8).

It should be noted that replacement of one thione in the $[Ag(PPh_3)_2(pymtH)_2]^+$ cation by a PPh_3 molecule to give the respective and stable tetrahedral $[Ag(PPh_3)_3(pymtH)]^+$ (**5**) complex results in a more positive charge (+0.20) for the metal center. In this regard, the additional triphenylphosphine can stabilize the accumulated electron density on the metal core through charge delocalization. This is better indicated by the strong involvement of the phosphine parts on the HOMOs of both the tetrahedral systems along with metal based AOs (Table S8). On the other hand, the pyrimidine ring is related to the vacant orbitals (LUMO) and thus cannot offer any charge relaxation on the metal core. On a totally similar basis the preferential formation of the $[Ag(PPh_3)_3(dmpymtH)]^+$ (**6**) complex over the $[Ag(PPh_3)_2(dmpymtH)_2]^+$ complex can be assigned to the same electronic factors described above and imposed by the replacement of a thione moiety by a PPh_3 ligand. The shape of the FMOs (Table S8) of these two complexes also supports the electronic stability offered by the presence of the phosphines

View Article Online
DOI: 10.1039/C4NJ02203C

through electron density delocalization. Despite the low positive charge of the metal center in both systems, the increase in the number of the coordinated phosphines causes a respective increase on its value by 100%.

Table 4. Selected principal singlet–singlet electronic transitions of the complex $[Ag(PPh_3)_2(pymtH)]^+$ (**7**) calculated at the PBE1PBE/6-31G(d),SDD level of theory.

Excitation	E/eV	λ/nm	Orbital Nature	Character	OS, f
HOMO → LUMO, HOMO-1 → LUMO	2.930	423	$4d_{Ag}/\pi_{PPh3} \rightarrow \pi^*_{(pymtH)}$	MLCT/LLCT	0.0030
HOMO-2 → LUMO, HOMO-4 → LUMO	3.523	352	$\pi_{PPh3} \rightarrow \pi^*_{(pymtH)}$	LLCT	0.0262
HOMO → LUMO+1	3.847	322	$4d_{Ag}/\pi_{PPh3} \rightarrow \pi^*_{(pymtH)}$	MLCT/LLCT	0.0408
HOMO-7 → LUMO	4.140	299	$\pi_{(pymtH)} \rightarrow \pi^*_{(pymtH)}$	IL	0.0010
HOMO-4 → LUMO+1, HOMO-2 → LUMO+1	4.576	271	$\pi_{PPh3} \rightarrow \pi^*_{(pymtH)}$	LLCT	0.0259
HOMO → LUMO+2, HOMO-1 → LUMO+2	4.677	265	$4d_{Ag}/\pi_{PPh3} \rightarrow \pi^*_{(PPh3)}$	MLCT/IL	0.0669
HOMO-1 → LUMO+3	4.767	260	$4d_{Ag}/\pi_{PPh3} \rightarrow 4d_{Ag}/\pi^*_{(PPh3)}$	MC/IL	0.2094
HOMO → LUMO+5	4.832	257	$4d_{Ag}/\pi_{PPh3} \rightarrow \pi^*_{(PPh3)}$	MLCT/IL	0.1007

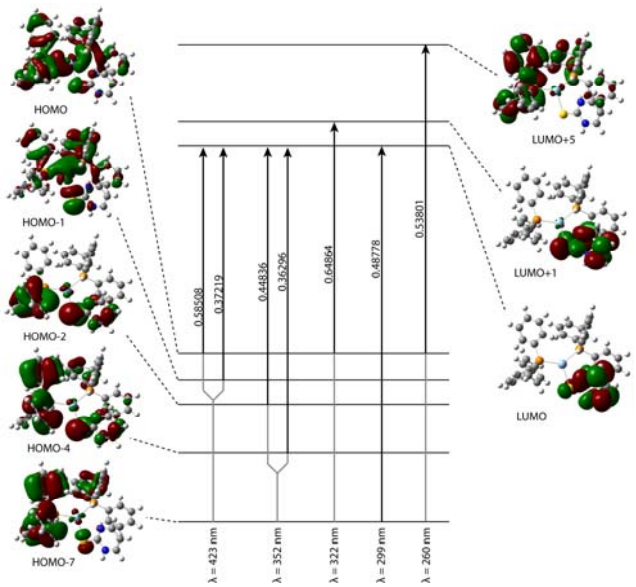

Figure 13. Predicted electronic transitions and participating MOs for the $[Ag(PPh_3)_2(pymtH)]^+$ (**7**) cation.

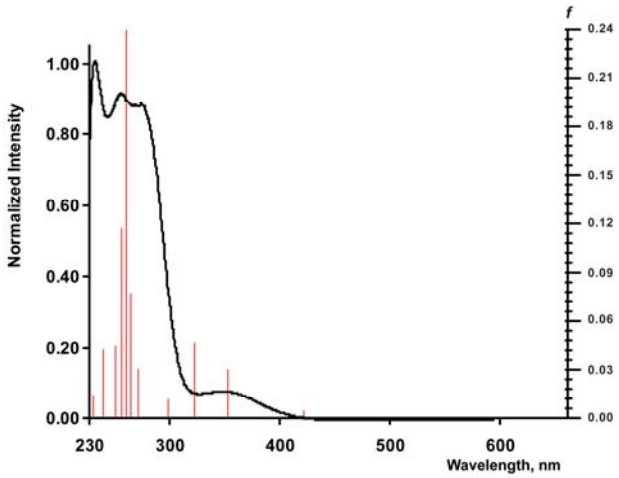

Figure 14. Experimental absorption spectrum of $[Ag(PPh_3)_2(pymtH)]^+$ (**7**) cation along with the calculated excitation energies appearing as vertical lines.

2.7.3 Electronic structure

In order to better clarify the electronic structure of the synthesized compounds, we report DFT results for a copper and a silver cation, namely $[Cu(PPh_3)_2(pymtH)_2]^+$ (**1**) and $[Ag(PPh_3)_2(pymtH)]^+$ (**7**), on the basis of MO shapes and excitation energies. A similar discussion is also presented for the $[Cu(PPh_3)_3(pymtH)]^+$ (**2**) cation as a means to probe differences resuting from the coordination of a PPh_3 moiety over a thione ligand. MO shapes for all of the optimized systems of interest are given in SI (Table S8) and are in agreement with the selected examples.

As already mentioned, the coordinated sulfur-ligands have been considered in their thione tautomeric form. The optimized geometries of the selected systems along with structural parameters are given in Tables S3 and S5 in SI. Concerning $[Cu(PPh_3)_2(pymtH)_2]^+$ (**1**) and $[Cu(PPh_3)_3(pymtH)]^+$ (**2**), a substantial difference occurs to the Cu-S and one of the Cu-P bond lengths for the two optimized geometries as a result of the sterically crowded environment in the 1:3:1 complex. This does not hold in the same extent for the two related dmpymtH systems.

In all cases the thione C=S bond lengths are found typically equal and agree well with crystallographic data.

As can be seen in Figures 11 and 12 the highest occupied orbital (HOMO) of both copper systems is of a d-σ character comprising mainly contributions from the metal center d AOs and the phosphine moieties. In the case of $[Cu(PPh_3)_2(pymtH)_2]^+$ (**1**) there is an additional slight participation from the π-system of one thione ligand. The same holds for HOMO-1 which retains a d-σ nature and extends over the same molecular parts. The sulfur atoms of the thiones also make some contributions to this orbital. On the other hand and in both cases the lowest virtual orbitals (LUMO and LUMO+1) can be assigned as π^*-MOs totally located on the heterocyclic thiones and being almost degenerate for the $[Cu(PPh_3)_2(pymtH)_2]^+$ (**1**) complex. Considering that the lowest energy excitations of the above Cu^I heteroleptic complexes will mainly involve transitions between the aforementioned MOs, it becomes apparent that their lowest lying singlet excited state can be assigned as a mixed Cu^I-to-thione and

View Article Online
DOI: 10.1039/C4NJ02203C

phosphine-to-thione charge transfer in nature (MLCT/LLCT).

Figure 13 and Table 4 comprise the shapes of MOs and the predicted vertical electronic transitions for the trigonal planar silver cation in its optimized structure. As in the case of copper compounds, HOMO is of a d-σ character bearing substantial contribution from the π-system of the two phosphines and smaller but important participation of the metal center d AOs as well as from the thione sulfur atom. Similarly HOMO-1 retains the d-σ nature extending typically over the same molecular parts although it mainly locates in the AgP_2S-core of the cation. The lowest virtual orbitals (LUMO and LUMO+1) can be assigned as π^*-MOs totally located on the heterocyclic thione ring with participation of the sulfur atom AOs. As is expected, the lowest energy excitations will mainly comprise transitions between the aforementioned FMOs. In this sense the lowest singlet excited state of silver systems can be also described as being of a mixed MLCT/LLCT character.

In Figure 14, a simulation of the experimental absorption spectrum of $[Ag(PPh_3)_2(pymtH)]^+$ (**7**) through TD-DFT calculations is presented. The computed eigenvectors offer a rather good description of the longer wavelength region with three basic excitations (423, 352, 322 nm) corresponding to the shoulder over 320 nm. According to the shape of the involved MOs (Table 2) these transitions are better assigned as MLCT/LLCT in nature embarking from the metal center and the phosphine moieties towards the vacant π-orbitals of the thione heterocyclic ring. Higher energy excitations are also in accord with experimental absorption bands and mainly comprise an MLCT/IL character. Similar calculations for $[Cu(PPh_3)_2(pymtH)_2]^+$ (**1**) also reveal a good representation of the experimental absorption spectrum by the derived vertical excitations and predict an MLCT/LLCT character for the lower energy transition of the system (Figure S4). The above results verify the quality of the selected level of theory on the description of the electronic structure of all the systems included in the present work.

2.7.4 Emission wavelength prediction

Further studies were undertaken in order to elucidate the nature of the emission observed for $[Cu(PPh_3)_3(dmpymtH)]^+$ (**4**) in the solid state. As already mentioned, this emission potently originates from a ^{3}MLCT state. In this context, two theoretical approximations have already been estabilised for the description of the photophysics of transition metal complexes behaving as triplet emitters.[48] One relays on the estimation of the energetics for the vertical T_1-S_o transition by calculating the energy difference (Δ-SCF) between the fully optimized T_1 state of the system and its ground state (S_o) retaining the T_1 geometry. The second method is more broadly applied and uses TD-DFT in order to predict the vertical electronic excitation energy between the closed-shell ground state of the system and its T_1 state using the T_1 structure.[48-50]

In general terms both methods are based on the optimal T_1 geometry since the vertical emissive de-excitation process occurs from this state, and usually refer to solution experimetal data where the molecule can easily undergo stuctural changes in order to obtain this geometry after photoexcitation. However, in the solid state the molecule is rather constrained and structural rearrangement is significantly restricted. In this framework, time-resolved X-ray diffraction studies on Cu^I complexes in the crystalline phase revealed only modest alterations of dihedral angles upon excitation with a concomitant diminishing of reorganization energies.[51,52]

Hence, in order to assign the emissive state of $[Cu(PPh_3)_3(dmpymtH)]^+$ (**4**) in the solid state, we performed TD-DFT calculations assuming negligible structural variations of the complex in the excited state. In this sense and by retaining the ground state geometry of the system, the energy for the vertical S_0-T_1 transition was estimated at 461 nm which is close to the determined 505 nm emission wavelength. Energy deviations can be attributed to the small, although expected, geometry relaxation of the complex after photoexcitation. It should be pointed that the proposed TD-DFT method for the prediction of the emission energy gives, in this case, a rather unrealistic result (720 nm) while the Δ-SCF energetic approximation assuming geometry relaxation in the T_1 state results in a 640 nm wavelength prediction. Consequently our approximation seems to offer a realistic description of the de-excitation process and supports further the assignement of the emissive state of $[Cu(PPh_3)_3(dmpymtH)]^+$ (**4**) in the solid state as a ^{3}MLCT.

3. Conclusions

A new family of four heteroleptic tetrahedral Cu^I as well as two tetrahedral and one trigonal planar Ag^I complexes, have been synthesized and structurally characterized. The isolation of the latter complex confirms previous findings.[36a] In all cases the sulfur-ligands are coordinated on the metal center in a monodentate mode through their thione-type S atom. Spectroscopic results along with theoretical data reveal an MLCT/LLCT as the lowest singlet excited state of the systems. Further, for all complexes in dichloromethane, a phosphine-derived emission is detected while in the solid state, $[Cu(PPh_3)_3(dmpymtH)]BF_4$ (**4**) emits at 505 nm from a ^{3}MLCT/LLCT excited state.

Theoretical calculations were also performed in order to rationalize the reasons leading to the unexpected stoichiometries for two of the synthesized Ag^I-complexes. The non feasible isolation of $[Ag(PPh_3)_2(pymtH)_2]^+$ and $[Ag(PPh_3)_2(dmpymtH)_2]^+$ cations may be explained by a predicted charge accumulation on the metal center which further results in strong repulsive forces towards the thione-ligands. The replacemcent of one thione by a PPh_3 molecule results to the stable tetrahedral $[Ag(PPh_3)_3(pymtH)]^+$ (**5**) and $[Ag(PPh_3)_3(dmpymtH)]^+$ (**6**) cations where an electron spreading towards the phosphine phenyl rings offers a charge relaxation on the metal core. This observation could be related to a stronger participation of the phosphine moieties on the high-lying occupied MOs compared to the heterocyclic thione ring. In this respect the non formation of the Ag:PPh_3:thione = 1:2:2 complexes can be attributed to electronic factors. On the other hand the compensation between a trigonal planar (Ag:PPh_3:thione = 1:2:1) and a Ag:PPh_3:thione = 1:3:1 tetrahedral complex can be rationalized on the basis of thermochemical data and steric demands.

Biological assesments showed that the two tetrahedral Ag^I complexes are characterized by a strong antimicrobial activity,

View Article Online
DOI: 10.1039/C4NJ02203C

while Cu^{I} compounds show selective action only against certain Gram-positive bacteria. On the other hand, only a moderate activity towards lixygenase inhibition was revealed, directly related to the bulkiness of the coordination sphere.

4. Experimental

4.1 Materials and measurements

The starting material $[Cu(MeCN)_4]BF_4$ was synthesized according to the proposed method.[53] $AgNO_3$, triphenylphosphine, pyrimidine-2-thione and 4,6-dimethyl-pyrimidine-2-thione were used as received. Solvents of reagent grade were also used without any prior purification or drying process. Elemental analyses for C, H and N were performed with a Perkin-Elmer 240B elemental analyzer. Infrared spectra were recorded in KBr pellets on a Nicolet FT-IR 6700 spectrophotometer. Electronic absorption spectra were recorded in 1 cm cuvettes on a Shimadzu 160A spectrophotometer. Emission studies in solution and in KBr disks were performed on a Hitachi F-7000 Fluorometer.

4.2 X-ray crystal structure determination

X-ray quality crystals of compounds **1**–**7** were grown from dichloromethane-chloroform and/or methanol solutions. For the structure determination of **1**–**2** and **4**–**7**, single crystals of the respective compounds were mounted on a Bruker Kappa APEX II diffractometer equipped with a triumph monochromator at ambient temperature. Diffraction measurements were made using graphite monochromated Mo Kα radiation. Unit cell dimensions were determined and refined by using the angular settings of at least 100 high intensity (>20σ(I)) reflections in the range $20<2\theta<40$ °. Intensity data were recorded using ϕ and ω scan modes. The frames collected for each crystal were integrated with the Bruker SAINT software package[57] using a narrow-frame algorithm. Data were corrected for absorption using the numerical method (SADABS) based on crystal dimensions.[58]

All structures were solved using the SUPERFLIP[59] package and refined by full–matrix least-squares method on F^2 using the CRYSTALS package version 14.40b.[60] All non-disordered non-hydrogen atoms have been refined anisotropically. For the disordered non-hydrogen atoms of the tetrafluoro borate and nitrate anions, occupancy factors were first determined with fixed isotropic displacements. Finally, all them were isotropically refined with fixed occupancy factors. All hydrogen atoms except the amine ones in **1** were found at the expected positions and refined using soft constraints. By the end of the refinement, they were positioned using riding constraints. In the case of **1**, both the pyrimidino nitrogen atoms in both pyrimidino-thione ligands have been found partially protonated with equal occupation factors.

X-ray diffraction data for compound **3** were collected by the NCS[61] on a Rigaku Saturn 724+ diffractometer. Radiation source: fine-focus sealed tube. Graphite monochromator, Mo Kα radiation. Profile data from ω scans. CrystalClear-SM Expert[62] was used for cell refinement, data collection and data reduction. The structure was solved with SHELXS97[63] and refined with SHELXL-97. The program used for molecular graphics was PLATON.[64] Tables for publication were prepared with SHELXS97 and WinGX.[65]

Crystal data and structure refinement parameters of **1**–**6** are presented in Table 1. Illustrations were drawn by CAMERON.[66] Further details on the crystallographic studies as well as atomic displacement parameters are given as Supporting Information in the form of cif files. CCDC-1019197 (**1**), CCDC-1019194 (**2**), CCDC-1018215 (**3**), CCDC-1019193 (**4**), CCDC-1019196 (**5**) and CCDC-1019195 (**6**) containing the supplementary crystallographic data for this paper. These data can be obtained free of charge at **www.ccdc.cam.ac.uk/conts/retrieving.html** [or from the Cambridge Crystallographic Data Centre, 12 Union Road, Cambridge CB2 1EZ, UK ; Fax: (intrnat.) + 44-1223/336-033; E-mail: **deposit@ccdc.cam.ac.uk**].

4.3 Materials and methods for biological tests

Culture media were prepared as described previously.[54] Four bacterial species were used for the antibacterial screening: *E. coli* (XL1), *S. aureus* (NCIM 2079), *B. subtilis* (ATCC 6633), and *B. cereus* (ATCC11778). The minimum inhibitory concentration (MIC) method uses the progressive double dilution in MMS, which contains the final concentrations of 50, 25, 12, 6, and 3 μg/mL of the complexes. The stock solutions of the complexes (10 mg/mL) were prepared by formerly dissolving in DMSO.

For the *in vitro* evaluation of lipoxygenase inhibition activity, the reaction mixture contained (final concentration) the test compounds, dissolved in 25% DMSO at concentrations of 50–500 μM, or the solvent (control), soybean lipoxygenase, dissolved in 0.9% NaCl solution (250 u/mL) and sodium linoleate (100 μM), in Tris–HCl buffer, pH 9.0. Lipoxidase from *Glycine max* (soybean) was used (L7395-15 MU, Sigma) and linoleic acid sodium salt (L8134-100 MG, Sigma). The reaction was monitored for 5-15 min at 28ºC, by recording the absorbance of a conjugated diene structure at 234 nm, due to the formation of 13-hydroperoxy-linoleic acid. The performance of the assay was checked using nordihydroguaiaretic acid as a reference.[55]

4.4 Computational Details

The geometry of the ligands and all the Cu^{I} and Ag^{I} cations was optimized with DFT theory under vacuum conditions and without symmetry constraints with the PBE1PBE[43] functional. The 6-31G(d)[45] and SDD[44] basis sets were selected respectively for the light elements and the metal core. TD-DFT calculations for $[Cu(PPh_3)_2(pymtH)_2]^+$ (**1**) and $[Ag(PPh_3)_2(pymtH)]^+$ (**7**) in the vacuum state were performed on the same level of theory and with the same basis set. In all cases computations were executed with the Gaussian 03W[56] package. Vibrational frequencies calculations ensured the obtained geometries are real minima in the potential energy hypersurfaces. Visualization of the obtained structures and MOs was performed with GaussView 5.0.

4.5 Synthesis of the complexes

All Cu^{I} complexes were prepared according to the following general procedure. In a solution of $[Cu(MeCN)_4]BF_4$ (0.5 mmol) in 20 mL of CH_2Cl_2 the appropriate amount of solid

View Article Online
DOI: 10.1039/C4NJ02203C

triphenylphosphine is added (1 mmol for the Cu:PPh_3:thione = 1:2:2 or 1.5 mmol for the Cu:PPh_3:thione = 1:3:1 complexes respectively) under stirring. After the solution turns clear the proper quantity (1 mmol or 0.5 mmol respectively) of the selected thione dissolved in 20 mL of methanol is added. In the case of pymtH the final solution was slightly heated. After stirring for 30 min the resulting solutions were filtered and left to stand in air at room temperature after the addition of a small amount of $CHCl_3$. Slow evaporation of the solvent gave the products in the form of crystals which were filtered off and dried in vacuo. Similarly in the case of silver, the same reactions were performed, only $AgNO_3$ was used instead. Also only methanol was used as a solvent.

4.5.1 $[Cu(PPh_3)_2(pymtH)_2]BF_4$ (1)

Orange solid. Yield 93 % (0.46 mmol, 0.42 g). Elemental Analysis: Calcd for $C_{44}H_{38}BCuF_4N_4P_2S_2$: C, 58.77; H, 4.26; N, 6.23. Found: C, 58.55; H, 4.32; N, 6.21. IR (KBr, cm^{-1}): 3122 (br, =N-H), 3071 (w, =C-H), 2853 (w), 1967 (w), 1910 (w), 1601 (s), 1571 (s), 1480 (s), 1434 (s), 1324 (s), 1179 (s), 1093 (s), 1060 (s, BF_4^-), 985 (m), 743 (s), 694 (s), 516 (s).

4.5.2 $[Cu(PPh_3)_3(pymtH)]BF_4$ (2)

Yellow solid. Yield 94 % (0.47 mmol, 0.49 g). Elemental Analysis: Calcd for $C_{58}H_{49}BCuF_4N_2P_3S$: C, 66.39; H, 4.71; N, 2.67. Found: C, 66.51; H, 4.68; N, 2.66. IR (KBr, cm^{-1}): 3119 (w, =N-H), 3051 (w, =C-H), 2850 (w), 1963 (w), 1913 (w), 1610 (s), 1583 (s), 1478 (s), 1434 (s), 1334 (s), 1179 (s), 1091 (s), 1064 (s, br, BF_4^-), 986 (m), 743 (s), 696 (s), 517 (s).

4.5.3 $[Cu(PPh_3)_2(dmpymtH)_2]BF_4$ (3)

Orange solid. Yield 93 % (0.46 mmol, 0.44 g). Elemental Analysis: Calcd for $C_{48}H_{46}BCuF_4N_4P_2S_2$: C, 60.35; H, 4.85; N, 5.86. Found: C, 60.32; H, 4.88; N, 5.82. IR (KBr, cm^{-1}): 3196 (br, =N-H), 3050 (w, =C-H), 2870 (w), 1970 (w), 1898 (w), 1618 (s), 1563 (s), 1480 (s), 1434 (s), 1324 (w), 1231 (s), 1185 (m), 1093 (s), 1061 (s, BF_4^-), 998 (s), 747 (s), 695 (s), 517 (s).

4.5.4 $[Cu(PPh_3)_3(dmpymtH)]BF_4$ (4)

Yellow solid. Yield 92 % (0.46 mmol, 0.49 g). Elemental Analysis: Calcd for $C_{60}H_{53}BCuF_4N_2P_3S$: C, 66.89; H, 4.96; N, 2.60. Found: C, 66.80; H, 4.91; N, 2.64. IR (KBr, cm^{-1}): 3139 (w, =N-H), 3051 (w, =C-H), 1967 (w), 1891 (w), 1618 (s), 1563 (s), 1479 (s), 1433 (s), 1234 (s), 1181 (w), 1091 (s), 1064 (s, br, BF_4^-), 997 (s), 745 (s), 695 (s), 517 (s).

4.5.5 $[Ag(PPh_3)_3(pymtH)]NO_3$ (5)

Yellow solid. Yield 92 % (0.46 mmol, 0.49 g). Elemental Analysis: Calcd for $C_{58}H_{49}AgN_3O_3P_3S$: C, 65.17; H, 4.62; N, 3.93. Found: C, 65.20; H, 4.59; N, 3.92. IR (KBr, cm^{-1}): 3072 (w, =N-H), 3048 (w, =C-H), 1963 (w), 1910 (w), 1610 (s), 1591 (s), 1478 (s), 1434 (s), 1338 (s, NO_3^-), 1177 (s), 1093 (s), 972 (m), 743 (s), 697 (s), 516 (s).

4.5.6 $[Ag(PPh_3)_3(dmpymtH)]NO_3$ (6)

Yellow solid. Yield 93 % (0.47 mmol, 0.51 g). Elemental Analysis: Calcd for $C_{60}H_{53}AgN_3O_3P_3S$: C, 65.70; H, 4.87; N, 3.83. Found: C, 65.72; H, 4.85; N, 3.82. IR (KBr, cm^{-1}): 3075 (w, =N-H), 3049 (w, =C-H), 1968 (w), 1912 (w), 1618 (s), 1565 (s), 1479 (s), 1433 (s), 1334 (s, NO_3^-), 1179 (s), 1093 (s), 997 (m), 742 (s), 693 (s), 514 (s).

4.5.7 $[Ag(PPh_3)_2(pymtH)]NO_3$ (7)

Yellow solid. Yield 95 % (0.48 mmol, 0.38 g). Elemental Analysis: Calcd for $C_{40}H_{34}AgN_3O_3P_2S$: C, 59.56; H, 4.25; N, 5.21. Found: C, 59.51; H, 4.26; N, 5.23. IR (KBr, cm^{-1}): 3120 (w, =N-H), 3063 (w, =C-H), 1967 (w), 1910 (w), 1602 (s), 1588 (s), 1477 (s), 1433 (s), 1337 (s, NO_3^-), 1172 (s), 1095 (s), 948 (m), 743 (s), 693 (s), 517 (s).

Acknowledgments

a) This research has been co-financed by the European Union (European Social Fund–ESF) and Greek national funds through the Operational Program "Education and Lifelong Learning" of the National Strategic Reference Framework (NSRF) - Research Funding Program: **ARCHIMEDES III**. Investing in knowledge society through the European Social Fund.

b) We thank the EPSRC UK National Crystallographic Service at the University of Southampton for the collection of the crystallographic data of compound **3**.

Notes and references

[a] *Aristotle University of Thessaloniki, Department of Chemistry, Laboratory of Inorganic Chemistry, P.O.B. 135, GR-541 24 Thessaloniki, Greece. Fax: +30 2310 997738; E-mail: panpapan@chem.auth.gr, hatzidim@chem.auth.gr, aslanidi@chem.auth.gr*

[b] *Aristotle University of Thessaloniki, Department of Chemistry, Laboratory of Applied Quantum Chemistry, P.O.B. 135, GR-541 24 Thessaloniki, Greece. Fax: +30 2310 997738; E-mail: anastp@chem.auth.gr*

[c] *Aristotle University of Thessaloniki, Department of Chemistry, Laboratory of Biochemistry, P.O.B. 135, GR-541 24 Thessaloniki, Greece; E-mail: natasa@chem.auth.gr*

[d] *School of Pharmacy, The Robert Gordon University, Schoolhill, Aberdeen AB10 1FR, Scotland, United Kingdom. Email: p.j.cox@rgu.ac.uk*

† Electronic Supplementary Information (ESI) available: crystallographic data and refinement details for the isolated complexes (Table S1), theoretical structural and energetic data in various media for pymtH and dmpymtH (Table S2), optimized structures and geometry parameters for the studied Ag^I and Cu^I cations (Tables S3-S6), NBO atomic charges for the ligands and the studied Ag^I complexes (Table S7), FMOs of the optimized stucture of all the studied Cu^I and Ag^I cations (Table S8), normalized absorption spectra of Cu^I-pymtH complexes and two of the isolated Ag^I-complexes in dichloromethane (Figure S1), normalized absoprtion and emission spectra of the ligands in dichloromethane (Figure S2), normalized emission spectra of all the isolated complexes in dichloromethane (Figure S3), selected excitations of the $[Cu(PPh_3)_2(pymtH)_2]BF_4$ (**1**) from TDDFT and simulation of the experimental absorption spectrum (Figure S4). See DOI: 10.1039/b000000x/

1. a) L. Dahlenburg and M. Kühnlein, Eur. J. Inorg. Chem., 2000, 2117-2125; b) P. Aslanidis, S. K. Hadjikakou, P. Karagiannidis, M. Gdaniec and Z. Kosturkiewicz, Polyhedron, 1993, 12, 2221-2226; c) P. Aslanidis, P. J. Cox, S. Divanidis, A. C. Tsipis, Inorg. Chem., 2002, 41, 6875-6886; d) W. McFarlane, P D. Akrivos, P. Aslanidis, P. Karagiannidis, C. Hatzisymeon, M. Numan, S. Kokkou, Inorg. Chim. Acta, 1998, 281, 121-125.

View Article Online
DOI: 10.1039/C4NJ02203C

2. P. J. Cox, P. Aslanidis, P. Karagiannidis, S. Hadjikakou, Inorg Chim Acta, 2000, 310, 268-272.
3. S. K. Hadjikakou, P. Aslanidis, P. Karagiannidis, D. Mentzafos, A. Terzis, Polyhedron, 1991, 10, 935-940.
4. S. K. Hadjikakou, P. Aslanidis, P. Karagiannidis, A. Aubry, S. Skoulika, Inorg. Chim. Acta, 1992, 193, 129-135.
5. P.J Cox, P.Aslanidis, P. Karagianidis, Polyhedron, 2000, 19 1615-1620.
6. P. Aslanidis, P. J. Cox, S. Divanidis, P. Karagiannidis, Inorg. Chim. Acta, 2004, 357, 4231-4239.
7. a) R. Lontie, Copper Proteins and Copper Enzymes, Vol I-III, CRC Press, Boca Raton, FL, 1984; b) W. L. Kwik, K. P. Ang, P. C. Lau, J. Chem. Soc. Dalton Trans., 1983, 2269-2272; c) A. A. Gewirth, E. I. Solomon, J. Am. Chem. Soc., 1988, 110, 3811-3819; d) N. Armaroli, G. Accorsi, F. Cardinali, A. Listorti, Top. Curr. Chem., 2007, 280, 69-115.
8. S. Jayasree, K. K. Aravindakshan, Synthesis and Reactivity in Inorganic, Metal-Organic and Nano-Metal Chemistry, 2005, 35, 855–863.
9. W. O. Foye, J. R. Lo, J. Pharm. Sc., 1972, 61, 1209-1212.
10. C. T. Dillon, T. W. Hambley, B. J. Kennedy, P. A. Lay, J. E. Weder, Q. Zhou, Metal Ions in Biological Systems, 2004, 41, 253-277.
11. D. H. Brown, W. E. Smith, J. W. Teape, A. J. Lewis, J. Med. Chem., 1980, 23, 729-734.
12. M. H. Shin, F. Y. Ke, Bioorg. Med. Chem., 2004, 12, 4633-4643.
13. E. Pontiki, D. Hadjipavlou-Litina, A. Chaviara and P. Papanikolaou, Curr. Res. Chem. Sci., 2013, 1, 11-16.
14. P. Aslanidis, P.J. Cox, S. Divanidis, P. Karagiannidis, Inorg. Chim. Acta, 2004, 357, 4231-4239.
15. E. S. Raper, Coord. Chem. Rev., 1994, 129, 91-156.
16. N. Cutillas, A. Martínez, G. S. Yellol, V. Rodríguez, A. Zamora, M. Pedreño, A. Donaire, C. Janiak, J. Ruiz, Inorg. Chem., 2013, 52, 13529-13535.
17. a) V. I. Prisakar, V. I. Tsapkov, S. A. Buracheéva, M. S. Byrké, A. P. Gulya, Pharm. Chem. J., 2005, 39, 313-315. b) P.C. Zachariadis, S. K. Hadjikakou, N. Hadjiliadis, S. Skoulika, A. Michaelides, J. Balzarini, E. De Clercq, Eur. J. Inorg. Chem., 2004, 1420–1426; c) K. Lazarou, B. Bednarz, M. Kubicki, I.I. Verginadis, K. Charalampopoulos, N. Kourkoumelis, S. K. Hadjikakou, Inorg. Chim. Acta, 2010, 363, 763–772; d) S. K. Hadjikakou, I. I. Ozturk, M. N. Xanthopoulou, P. C. Zachariadis, S. Zartilas, S. Karkabounas, N. Hadjiliadis, J. Inorg. Biochem., 2008, 102, 1007–1015; e) G.K. Batsala, V. Dokorou, N. Kourkoumelis, M.J. Manos, A.J. Tasiopoulos, T. Mavromoustakos, M. Simcic, S. Golic-Grdadolnik, S.K. Hadjikakou, Inorg. Chim. Acta, 2012, 382, 146 – 157.
18. a) P. Aslanidis, P. J. Cox, K. Kapetangiannis, A. C. Tsipis, Eur. J. Inorg. Chem., 2008, 5029-5037; b) M. G. Babashkina, D. A. Safin, A. Klein, and M. Bolte, Eur. J. Inorg. Chem., 2010, 4018-4026.
19. P. Aslanidis, P. J. Cox, A. C. Tsipis, Dalton Trans., 2010, 39, 10238-10248.
20. I. Papazoglou, P. J. Cox, A. G. Papadopoulos, M. P. Sigalas, P. Aslanidis, Dalton Trans., 2013, 42, 2755-2764.
21. V. W. W. Yam, C. H. Lam, W. K. M. Fung, K. K. Cheung, Inorg. Chem., 2001, 40, 3435-3442.
22. V. W. W. Yam, W. K. Lee, T. F. Kai, J. Chem. Soc. Chem. Commun., 1993, 1571-1573.
23. R. Langer, M. Yadav, B. Weinert, D. Fenske, O. Fuhr, Eur. J. Inorg. Chem., 2013, 3623-3631.
24. a) H. W. Gardner, Biochimica Biophysica Acta, 1991, 1084, 221-239. b) G. P. Pidgeon, J. Lysaght, S. Krishnamoorthy, J.V. Reynolds, K. O'Byrne, D. Nie, K. V. Honn. Cancer Metastasis Rev., 2007, 26, 503-524. c) B. S. Zweifel, M. M. Hardy, G. D. Anderson, D. R. Dufield, R. A. Pufahl, J. L. Masferrer, Eur J Pharmacol., 2008, 584, 166-174.
25. J. Guillermo Contreras and J. B. Alderete, J. Mol. Struct. (THEOCHEM), 1991, 231, 257-265 and refs cited therein.
26. M. C. P. Lima, K. Coutinho, S. Canuto and W. R. Rocha, J. Phys. Chem. A, 2006, 110, 7253-7261.
27. D. W. Aksnes, H. Kryvi, Acta Chem. Scand., 1972, 26, 2255-2266.
28. M. J. Nowak, H. Rotkowska, L. Lapinski, J. leszczynski, J. S. Kwiatkowski, Spectrochim. Acta, 1991, 47A, 339-353.
29. D. Moran, K. Sukcharoenphon, R. Puchta, H. F. Schaefer, III, P. v. R. Schleyer, and C. D. Hoff, J. Org. Chem., 2002, 67, 9061-9069.
30. P. Viswanathamurthi and M. Muthukumav, J. Chem. Sci., 2011, 123, 567-576.
31. P. A. Papanikolaou, P. C. Christidis, A. Th. Chaviara, C. A. Bolos, and A. C. Tsipis, Eur. J. Inorg. Chem., 2006, 2083-2095.
32. R. Allman, M. Krestl, C. Bolos, G. Manoussakis, G. St. Nikolov, Inorg. Chim. Acta, 1990, 175, 255–260.
33. P. Karagiannidis, P. Aslanidis, S. Papastefanou, D. Mentzafos, A. Hountas, A. Terzis, Inorg. Chim. Acta, 1989, 156, 265–270.
34. Karagiannidis, P. Aslanidis, S. Papastefanou, D. Mentzafos, A. Hountas, A. Terzis, Polyhedron, 1990, 9, 2833–2837.
35. C. Ntoras, P.J. Cox, P. Aslanidis, Polyhedron, 2012, 34, 171-175.
36. a) P. Aslanidis, P. Karagiannidis, P. D. Akrivos, B. Krebs, M. Läge, Inorg. Chim. Acta, 1997, 254, 277-284; b) A. G. Young, L. R. Hanton, Coord. Chem. Rev., 2008, 252, 1346-1386.
37. A. A. Del Pagio, D. R. McMillin, Inorg. Chem., 1983, 22, 691-692.
38. C. Kutal, Coord. Chem. Rev., 1990, 90, 213-253.
39. P. J. Cox, A. Kaltzoglou, P. Aslanidis, Inorg. Chim. Acta, 2006, 359, 3183-3190.
40. H. Kunkely, A. Vogler, Inorg. Chim. Acta, 2006, 359, 383-390.
41. a) N. Armaroli, Chem. Soc. Rev., 2001, 30, 113-124. b) P. Changenet, P. Plaza, M. M. Martin,Y. H. Meyer, W. Rettig, Chem. Phys., 1997, 221, 311-322.
42. H. Kunkely, A. Vogler, Inorg. Chem. Commun., 2004, 7, 400-401.
43. a) J. P. Perdew, K. Burke and M. Ernzerhof, Phys. Rev. Lett., 1996, 77, 3865-3868; b) J. P. Perdew, K. Burke and M. Ernzerhof, Phys. Rev. Lett., 1997, 78, 1396-1396.
44. a) A. Bergner, M. Dolg, W. Kuechle, H. Stoll, H. Preuss, Mol. Phys., 1993, 80, 1431-1441; b) M. Kaupp, P. v. R. Schleyer, H. Stoll, H. Preuss, J. Chem. Phys., 1991, 94, 1360-1367; c) M. Dolg, H. Stoll, H. Preuss, R. M. Pitzer, J. Phys. Chem., 1993, 97, 5852-5859; d) D. Andrae, U. Haussermann, M. Dolg, H. Stoll, H. Preuss, Theor. Chim. Acta, 1990, 77, 123-141.
45. a) P. C. Hariharan, J.A. Pople, Theor. Chim. Acta, 1973, 28, 213-222; b) M. M. Francl, W. J. Petro, W. J. Hehre, J. S. Binkley, M. S. Gordon, D. J. DeFrees, J. A. Pople, J. Chem. Phys., 1982, 77, 3654–3665.
46. P. A. Papanikolaou, M. Gdaniec, B. Wicher, P. D. Akrivos and N. V. Tkachenko, Eur. J. Inorg. Chem., 2013, 5196-5205 and references cited therein.
47. S. Dapprich, G. Frenking, J. Phys. Chem., 1995, 99, 9352-9362.
48. Y. Unger, T. Strassner, C. Lennartz, J. Organomet. Chem., 2013, 748, 63-67 and refs cited therein.
49. T. Guillon, M. Boggio-Pasqua, F. Alary, J. L. Heully, E. Lebon, P. Sutra, A. Igau, Inorg. Chem., 2010, 49, 8862-8872.
50. L. Yang, J.-K. Feng, A.-M. Ren, M. Zhang, Y.-G. Ma, and X.-D. Liu, Eur. J. Inorg. Chem., 2005, 1867-1879.

View Article Online
DOI: 10.1039/C4NJ02203C

51. P. Coppens, I. I. Vorontsov, T. Graber, A. Y. Kovalevsky, Y. S. Chen, G. Wu, M. Gembicky, and I. V. Novozhilova, J. Am. Chem. Soc., 2004, 126, 5980-5981.

52. I. I. Vorontsov, T. Graber, A. Y. Kovalevsky, I. V. Novozhilova, M. Gembicky, Y. S. Chen, and P. Coppens, J. Am. Chem. Soc., 2009, 131, 6566-6573.

53. P. Hemmerich, C. Sigwart, Experentia, 1963, 19, 488.

54. a) D. N. Williams, S. H. Ehrman, T. R. P. Holoman, J. Nanobiotechnol., 2006, 4:3. b) M. A. Tsiaggali, E. G. Andreadou, A. G. Hatzidimitriou, A. A. Pantazaki, P. Aslanidis, J. Inorg. Biochem., 2013, 121, 121-128.

55. I. B. Taraporewala, J. M. Kauffman, J. Pharmaceut. Sci., 1990, 79, 173.

56. M. J. Frisch, G. W. Trucks, H. B. Schlegel, G. E. Scuseria, M. A. Robb, J. R. Cheeseman, J. A. Montgomery, Jr., T. Vreven, K. N. Kudin, J. C. Burant, J. M. Millam, S. S. Iyengar, J. Tomasi, V. Barone, B. Mennucci, M. Cossi, G. Scalmani, N. Rega, G. A. Petersson, H. Nakatsuji, M. Hada, M. Ehara, K. Toyota, R. Fukuda, J. Hasegawa, M. Ishida, T. Nakajima, Y. Honda, O. Kitao, H. Nakai, M. Klene, X. Li, J. E. Knox, H. P. Hratchian, J. B. Cross, C. Adamo, J. Jaramillo, R. Gomperts, R. E. Stratmann, O. Yazyev, A. J. Austin, R. Cammi, C. Pomelli, J. W. Ochterski, P. Y. Ayala, K. Morokuma, G. A. Voth, P. Salvador, J. J. Dannenberg, V. G. Zakrzewski, S. Dapprich, A. D. Daniels, M. C. Strain, O. Farkas, D. K. Malick, A. D. Rabuck, K. Raghavachari, J. B. Foresman, J. V. Ortiz, Q. Cui, A. G. Baboul, S. Clifford, J. Cioslowski, B. B. Stefanov, G. Liu, A. Liashenko, P. Piskorz, I. Komaromi, R. L. Martin, D. J. Fox, T. Keith, M. A. Al-Laham, C. Y. Peng, A. Nanayakkara, M. Challacombe, P. M. W. Gill, B. Johnson, W. Chen, M. W. Wong, C. Gonzalez and J. A. Pople, Gaussian 03, Revision E.01-SMP, Gaussian, Inc., Pittsburgh PA, 2003.

57. Bruker Analytical X-ray Systems, Inc. Apex2, Version 2 User Manual, M86-E01078, Madison, WI. 2006.

58. Siemens Industrial Automation, Inc. SADABS: Area-Detector Absorption Correction; Madison, WI. 1996.

59. P.W. Betteridge, J. R. Carruthers, R. I. Cooper, K. Prout, D.J. Watkin, J. Appl. Cryst., 2003, 36, 1487.

60. L. Palatinus, G. Chapuis, J. Appl. Cryst., 2007, 40, 786–790.

61. S. J. Coles, P.A. Gale, Chemical Science, 2012, 3, 683–689.

62. Rigaku, CrystalClear-SM Expert Rigaku Corporation, Tokio, Japan, 2011.

63. G. M. Sheldrick, Acta Crystallogr., Sect. A: Found. Crystallogr., 2008, 64, 112-122.

64. A. L. Spek, Acta Cryst. D, 2009, 65, 148–155.

65. L. J. Farrugia, J. Appl. Crystallogr., 1999, 32, 837–838.

66. D.J. Watkin, C.K. Prout, Pearce, L.J. CAMERON, Chemical Crystallography Laboratory, Oxford, UK. 1996.